DOI: 10.21062/mft.2026.022 http://www.journalmt.com

Spinning Bath Evaporator Availability and Reliability Enhancement Proposal

Jan Palátka (0009-0007-6178-4178), Karel Mayer, Martin Pexa (0000-0003-2872-3844), Eva Olmrová (0009-0001-1983-7463)
Faculty of Engineering, Czech University of Life Sciences. Kamýcká 129, 165 00, Prague, Czech Republic. E-mail: palatka@tf.czu.cz

A single-stage evaporator with natural circulation was used to densify the plasticizing bath through continuous evaporation and to prepare a solution used in the production of viscose fiber. During the process, sodium calcium sulfate salts were formed, leading to fouling of the heat transfer surfaces in the heat exchangers. This fouling created a layer of deposits that gradually reduced the efficiency of the evaporation process in the evaporator. It was determined that a processing medium with a volumetric flow rate of 6 $m^3 \cdot h^{-1}$ required a heat exchanger power of 1448 kW. A fouling layer with a thickness of 0.1 mm reduced the heat exchanger's performance by approximately 40%. When the fouling layer increased to 0.5 mm, the heat exchanger power decreased by nearly 74%, down to 889 kW. The purpose of this paper was to analyze the process parameters of the densification technology in order to identify potential optimizations that could increase equipment availability and reliability. Alternatively, the study aimed to provide recommendations for design modifications to the existing technology.

Keywords: Viscose, Evaporator, Fouling, Efficiency, Reliability

1 Introduction

Evaporator is a heat transfer device. Thermal requirement is one of the most important design factors. As a matter of fact, is has thermal requirements defined by conventional heat and material balance calculations. Heating surfaces are areas in direct contact with vaporized medium. Various issues resulting from design itself can be stated. They are likes of heat transfer, vapor and liquid separation, evaporator type selection related to a specific application and product quality, etc. From evaporator types and applications standpoint there is following distribution. There are evaporators, where the heating medium is separated from the evaporating liquid by tubular heating surfaces. Another type are evaporators whereby the heating medium is bounded by spirals, double walls, flat plates, etc. Then evaporators where the heating medium is brought into direct contact with the vaporized medium. And finally, evaporators that are heated by solar radiation. This article is a case of water vapor evaporator for heating, where heat comes in contact with the vaporized medium through tubular heat exchange surfaces. In case of the mentioned application it applies that there are several issues with reliability and performance due to initial selection of the evaporator type related to the application. The objective of this article is to provide a proposal for evaporator optimization in order to achieve better reliability and availability of the technology. There are two basic approaches to control evaporation. One of them is rate of evaporation and resulting concentration of the product. The rate of evaporation usually is achieved by controlling steam throughput. The conventional method is to use control instrumentation. Resulting product concentration can be controlled by any property of the solution that can be measured with the required accuracy and reliability. Generally preferred method is to introduce control of the evaporation rate of the product. The flow rate of the liquid medium into evaporator is subsequently controlled by level of evaporation rate. When this method is not achievable, it is often used to control the inflow rate of the product concentration by means of a steam inlet with a dosage related to the concentration of the evaporated product, or possibly by inlet concentration of the product. Other control mechanisms can also be considered, or even other control mechanisms due to feedstock or process conditions may differ.[1]

Evaporator in this case (fig. 1) is a technology used to densify spinning bath by continuous evaporation of plasticizing bath. Main target to achieve are required parameters for spinning bath. [2] Spinning bath gets used for viscose fiber manufacturing. [3] The technology used is a single-stage evaporator with natural circulation. [4] Heat transfer between water steam and plasticizing bath is carried out in an external heat exchanger. [5] Depending on time length of evaporator operation, a significant amount of fouling is formed on the heat transfer surfaces of heat exchangers. From a chemical perspective the fouling is $Na_2Ca(SO_4)_2$. These salts deposit in the heat

exchanger bundle and significantly reduce efficiency of the evaporation process over time.[6] After the efficiency drops below acceptable threshold, the operation of heat exchanger has to be discontinued and subsequently it is subjected to cleaning.[7] During the cleaning period, there is a backup heat exchanger that operates in the meantime. Described process is repeated cyclically. The purpose of this manuscript is a proposal for either process optimization or technology modification to increase availability, reduce maintenance costs and increase reliability of the technology.[8]

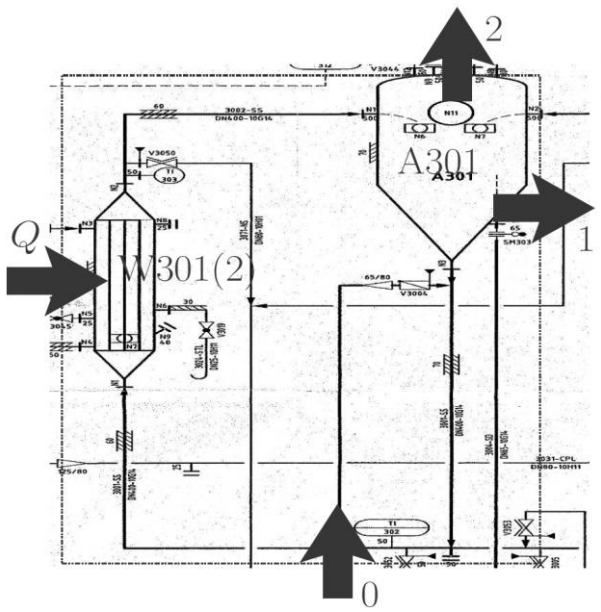

Fig. 1 *PID of evaporator technology [9]*

2 Technological description

Evaporator A301 is a pressure vessel (fig. 2) with a conical bottom and internal rubber coating. The inner diameter of the vessel is 2400 mm with a total height of 3035 mm. The densified solution is flowing into heat exchangers W301 and 302, it then returns through N1 / N2 pipe back to evaporator.

Level of densified solution is maintained in the vessel by an overflow pipeline. The densified solution flows out of the evaporator through N5 nozzle. Hydrostatic pressure plays significant role in terms of boiling point in W301 and W302 heat exchangers. Returning liquid is not fed in below surface level, rather than it flows in from above. The circulation loop is not closed. There is no nozzle in the evaporator, and therefore the liquid does not expand when entering evaporator. Heat exchangers W301 and W302 are vertical shell and tube bundles. The connection ports of the heated dilute solution are marked N1 / N2. Heat exchangers consist of graphite tubes with an inner diameter of 25 mm and an outer diameter of 37 mm. The heat exchanger bundle has a total of 280 pipes and is divided into 4 sections. Each section contains 70 pipes. Total length of the pipe is 4000 mm. Due to the tube housing design; the effective length of the heat exchanger pipe is 3834 mm. Total heat exchange surface of device is 85 m^2. Pipes and heat exchanger covers are made of steel S235JRG2, while the heat exchanger body is made of steel 1.4571. Surfaces used for direct contact with the process medium have a special polyvinylidene fluoride coating (PVDF). The surface treatment is important to prevent media contact with steel structure of the device. In case of incidental contact, chemical corrosion of the base material would occur [10], which is closely described in the upcoming chapter. The solution inflow into heat exchanger has lower temperature than its boiling point and corresponding enthalpy. Such solution is called a plasticizing bath. The plasticizing bath flows out of vessel A301 and is mixed with the inflowing dilute solution at temperature T_0, which corresponds to the specific enthalpy h_0.[11] The resulting enthalpy is given by the mixing of both streams.[12] The solution leaving evaporator has a specific enthalpy of the boiling solution. As a result, part of the aqueous component of the solution evaporates, resulting in a densified solution.[13] Part of the already densified solution is returned in the loop and the whole process is repeated as a new dilute solution inflows into the evaporator. Part of the densified solution continues downstream, whereby it is further adjusted to the required parameters using subsequent processes and ultimately it gets used as a spinning bath in the cord fiber spinning mill.

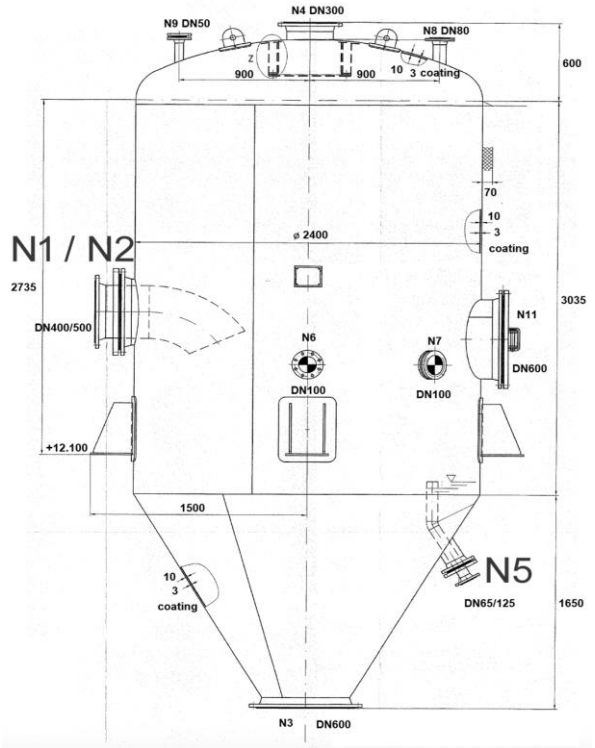

Fig. 2 *Drawing of the evaporator vessel*

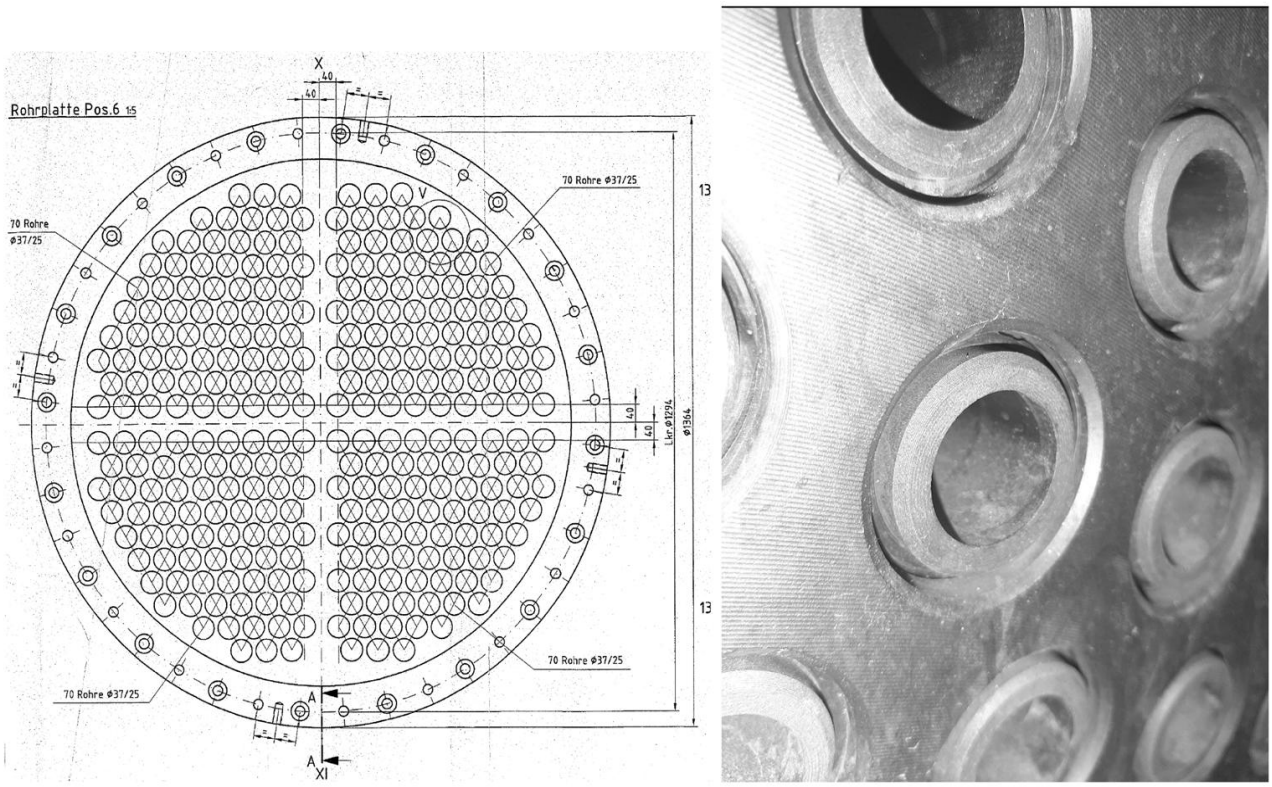

Fig. 3 *Front view of the W301 and W302 heat exchanger tube bundle with PVDF coating*

These shell and tube heat exchangers have PVDF-coated tube shells, which is similar to teflon (fig. 3). However, the material has a significant advantage in robust chemical resistance, heat resistance, abrasion resistance and high mechanical integrity. [14,15,16] As a result of thermal expansion, cyclic fatigue damage occurs to the tubes in the heat exchanger.[17] If there is a mechanical damage to the PVDF coating, chemical corrosion of the base material of the exchanger occurs. All the mentioned processes result in various maintenance activities, equipment repairs and related operational unavailability of the technology.[18] The resistance of a PVDF coating against acids and chemicals depends on two causes of degradation, physical and chemical. Physical, i.e. mechanical, degradation means the inevitable diffusion of chemicals into and through the protective coating.[19] The reaction of the base material components with the environment is classified as chemical degradation. [20] Physical and chemical degradation occur either separately or simultaneously, i.e. physical diffusion followed by chemical interactions. An important property of the acid-resistant coating is to remain inert to any reaction with sulfuric acid or any other additive that tends to damage the coating and cause premature failure, such as cracks exposing the base material. [21] In the long-term operation of heat exchangers, slow and time-related fouling is one of the most critical problems that seriously affects serviceability.[22]

3 Fouling

Due to periodical occurrence of deposits on the heat exchanger's inner surfaces, there is the aforementioned backup heat exchanger present. In case of need for cleaning, the backup heat exchanger gets put into operation. Fouling appears regularly in the pipes, tube sheets and heat exchanger bottoms [23], i.e. in the space of process media.[24] Reduction of heat output efficiency due to increased fouling on the heat exchange surfaces caused by precipitation of sodium calcium sulfate salts (or so-called glauberite), can be partially reduced by systematic increase of steam pressure and temperature. Which, as a result, means an increase in steam consumption. Thus, the amount of heating steam initially depends on the amount of the inflowing dilute solution of the plasticizing bath, but over time the amount of steam must be increased due to increasing fouling. Based on that, as a result certain extension of the cleaning interval may be achieved. The amount of heat that needs to be supplied to evaporator to ensure desired amount of water evaporates from the inflowing dilute solution has to be transferred through the heat transfer surface of the heat exchanger. It thus depends on the size of the heat exchanger, temperature conditions in the heat exchanger and the heat transfer mechanism.[25] In the beginning part of the heat exchanger tube, the solution is heated to the point of saturation. This is technically

a transfer of convection during flow of liquid through a pipe of circular cross-section.[26] The temperature of solution subsequently continues to rise until it reaches the boiling point temperature corresponding to the pressure at the given location. However, after a certain period of time, there is a layer of glauberite begins to form on the inner surface of the heat exchange surface. For this reason, the so-called fouling factor is introduced,[24] which is an operational index to measure the adverse effect of solids deposition on heat transfer capability.[27] The rate of formation of glauberite deposits on the inner surface of the heat exchanger is basically determined by two factors, as shown in fig. 4. Like any chemical reaction, the rate of growth of the deposit thickness is mainly determined by a temperature. The second factor affecting rate of deposit thickness formation is liquid flow velocity through the heat exchanger.[28] According to Hang et al. 2022 (fig. 4), fouling formation is primarily dependent on the temperature of heat transfer surface. The resulting deposits can be removed from the surface before they settle, and the removal rate depends on the flow rate of the flowing medium. If the settling rate is higher than the flow rate of the flowing medium, significant fouling can occur. Otherwise, negligible deposit formation can be expected. [29]

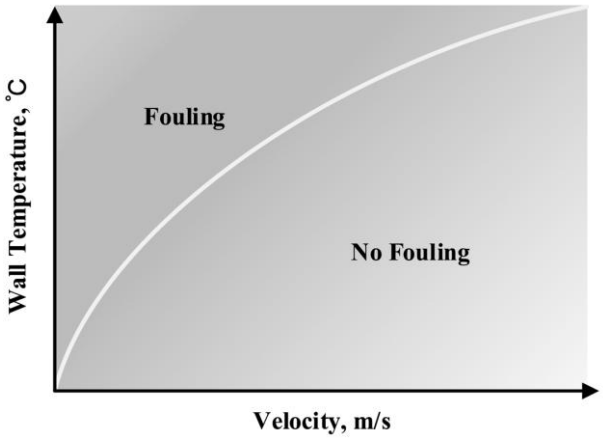

Fig. 4 *Threshold for fouling deposits formation [29]*

4 Chemical wear

The mechanism of chemical wear can be characterized as electrochemical corrosion in an aqueous environment. [30] The corroding metal in the liquid is anode. Corrosion is only possible when resulting electrons from the reaction are consumed by the cathodic reaction. Electrically, there is a conductive path between these two locations for electrons to pass through.[31] The first form of localized corrosion is pitting corrosion.[32] The PVDF protective coating protects the metal against electrochemical corrosion. The problem arises with mechanical defects of this protective layer, when pits are initiated, and these grow over time. Locally high acidity is a reason for the rapid development of a defect in the structural steel of tube sheets or exchanger covers.[33] This phenomenon can cause significant weakening of the structure, which could compromise structural integrity of the device. [34] A significant proportion of the heat exchange surface is made by graphite, which is not susceptible to chemical degradation by the medium. Thus chemical wear mechanism does not occur in pipes, which is a consequence of a fact that graphite in its impermeable form is very inert to a wide range of chemical environments, including acids, salt solutions and organic compounds. And spinning bath is no exception. This ensures high reliability and resistance to the harsh environment present in the technology. Therefore, the pipe installation is not a critical area from the point of view of chemical degradation. Also from the design standpoint of the heat exchanger, the corrosive medium does not flow through the shell, which guarantees there is no corrosion in the shell due to presence of a chemical environment.[35] Its chemical resistance combined with excellent heat transfer properties makes impermeable graphite a very popular material choice for heat exchangers. The disadvantage of this material lies in its relatively low tensile strength, which is also a source of mechanical defects, as is described in the following chapter. Threshold oxidation temperature for graphite is 400 °C, which is not achievable in the discussed technology. [36] Temperature of the spinning bath varies in between 120 – 130 °C.

5 Mechanical wear

Mechanical cyclic stress comes from several sources. One of them is the mentioned regular start-ups and discontinuing of the technology due to maintenance and especially activities related to the fouling removal. Due to that there are changes in operating temperatures and pressures inside the heat exchanger. As a result of thermal expansion of pipes, which are made of graphite not having high tensile strength, cracks may occur.[37] Fatigue defects occur in the heat exchanger due to its complex construction and harsh operating conditions. Fracture defects may also appear in weld joints. Quality of the weld joint significantly affects safety and reliability of equipment operation.[38] It is known that quality of welded joints may be affected not only by the welding process, but also by thermal expansion.[39] Likes of defects can cause high stress concentration; reduce contact area of the weld joint and reduce its fatigue performance. In fact, weld defects such as non-fusible weld defects could be considered initial cracks in the components.[40] These cracks can spread further.[41]

Periodic loading is a necessary condition for propagation of fatigue cracks.[42] Another source of periodic loading may come from resonant vibrations of the tubes, which could be caused by periodic fluid shocks.[43] Combined with the existence of initial defects and cracks in the weld joint, fatigue failure eventually occurs. [44] Another mechanism of mechanical wear is the failure of PVDF protective coating, caused by glauberite removal. Or even surface treatment defect caused by insufficient surface preparation during the technological coating process. Or perhaps due to bad or insufficient properties and inadequate composition of coating, which can lead to erosion, chalking and cracking of coating.[45] Alternatively, defects stemming from non-compliance with heat treatment technological process.[46] These aspects can lead to mechanical damage to the surface protection due to the abrasive properties of processed medium. [21]

6 Methodology

Data collection had been performed during the entire operating cycle of W301 heat exchanger. The collection had been carried out using process measuring instruments FIC314, TIC318, PI207, PICAH312, TI302, FIC301. Figure 5 shows a technological diagram with location of mentioned measuring instruments within the technology. A detailed description of instrumentation. Currently, it is necessary to increase steam temperature over time, which makes it possible to compensate to some extent for the decreasing performance in the heat exchanger due to growing deposit formation on the heat exchange surfaces. Flow rate of the dilute solution is variable, but most often 4 – 6 m^3h^{-1}. Amount of evaporated water is approximately 1.4 $t \cdot h^{-1}$, purely depending on the operating condition of evaporator. The amount of steam supplied to the heat exchanger is approximately 2 $t \cdot h^{-1}$. Spinning bath flows at a temperature of approximately 53.5 °C, with density of approximately 1200 $kg \cdot m^{-3}$. The aim of the process is to densify the solution to a density of approximately 1300 $kg \cdot m^{-3}$ at temperature of approximately 55 °C. Saturated steam temperature which supplies thermal energy to the technology has around 130 °C when entering the heat exchanger. Considering above conditions provided, the temperature of plasticizing bath solution is around 106 °C at the inlet. It then reaches a temperature of around 111 °C at the outlet. Currently time between setting clean heat exchanger for operation and its complete clogging with a layer of glauberite salt $Na_2Ca(SO_4)_2$ is around one month. After that, the heat exchanger is heavily contaminated with deposits in the inner space of the tube bundle and in both tube sheet fronts. If efficiency starts to drop due to fouling, this can partially be addressed by heating steam temperature and pressure increase adjusting the FV314 valve on the heat exchanger inlet is given below in relevant subsection.

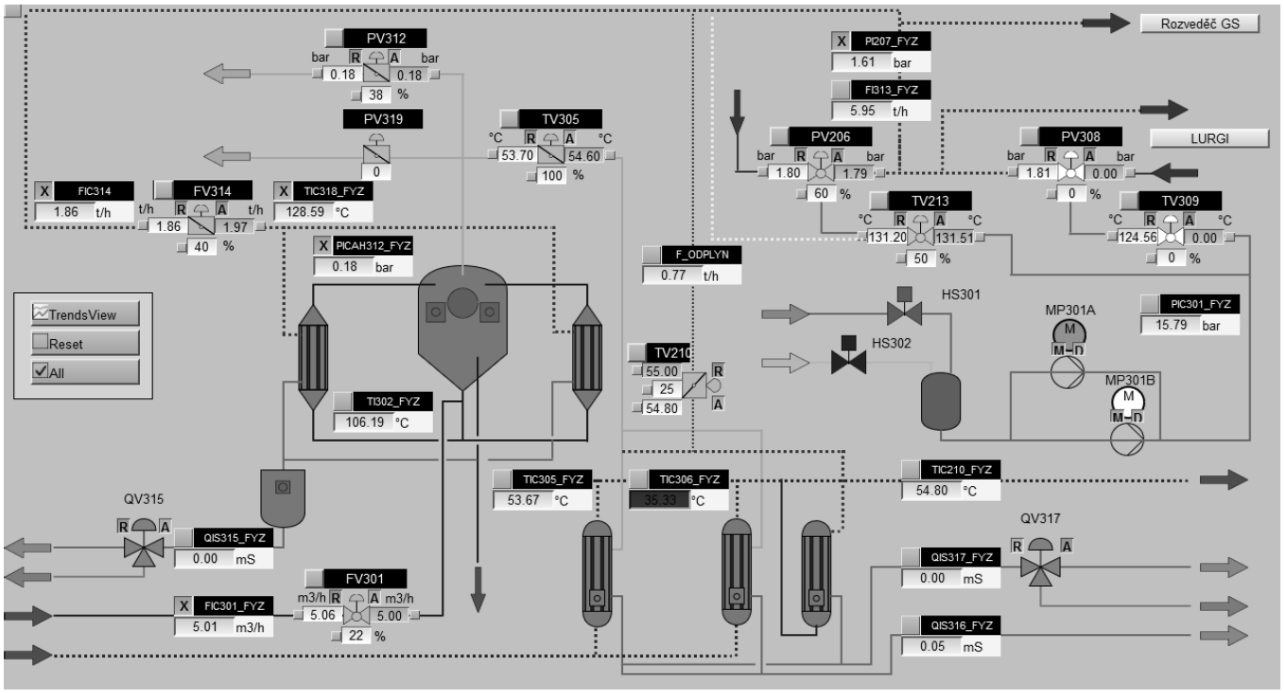

Fig. 5 *Technological diagram with indication of measuring points (SCADA)*

The solution composition as stated in table 1, where mass fraction values had been calculated for the inflow dilute solution with specific density of 1200 $kg \cdot m^{-3}$ and outflow densified solution with specific density of 1300 $kg \cdot m^{-3}$. [9]

Tab. 1 *Mass concentrations and mass fractions of individual components in the aqueous solution at the inlet and outlet of the evaporator [47]*

	Inlet		Outlet	
	ρ_0 [kg·m^{-3}]	ω_0 [%]	ρ_1 [kg·m^{-3}]	ω_1 [%]
H_2SO_4	80	6.67	128	9.85
Na_2SO_4	160	13.33	240	18.46
$ZnSO_4$	61	5.08	96	7.38
∑	301	25.08	464	35.69

7 Instrumentation

FIC314 measures mass flow of steam into the evaporator. It is an electromagnetic flow measurement according to Faraday's law using an Endress Hauser Promag 33F flowmeter with measurement deviation ± 0.2 %.[48]

TIC318 measures steam temperature at the inlet to the heat exchanger W301. It is temperature of saturated steam after FV314 reduction. The device is a resistance temperature measurement using a temperature sensor JSP PT100/B/4, type T10253 011 116 J10 N1 H3 P9, S/N 11009827 with measurement deviation ± 0.3 + 0.005 °C. [49]

PI207 measures steam pressure at the inlet to the heat exchanger. It is a resistance temperature measurement using a temperature sensor JSP PT100/B/4, type T10013 06F1 116 J10 N1 H3 P9, S/N 11112144 with measurement deviation ± 0.3 + 0.005 °C. [49]

PICAH312 measures pressure in the evaporator, at which the spinning bath solution evaporates. It is a process pressure sensor 4 to 20 mA Endress Hauser Promag Cerabar M PMP48, S/N 7300B901025 with measurement deviation ± 0.2 %. [50]

TI302 measures temperature of the solution in the evaporator. It is a resistance temperature measurement using a temperature sensor JSP PT100/B/2, type T10043 041 999 J10, S/N 110 29054 with measurement deviation ± 0,3 + 0,005 °C. [49]

FIC301 measures volumetric flow of the dilute spinning bath solution at the inlet to the evaporator. It is an electromagnetic flow measurement according to Faraday's law using a meter Endress Hauser Promag 33F DN50 PN40, S/N OZ 439043 with measurement deviation ± 0.2 %.[48]

8 Mass and enthalpy balance of the evaporator

As shown in fig. 5, where a basic technological schematic can be found, there are inlet and outlet streams to the evaporator and heat exchangers through which steam flows and supplies heat Q. The dilute solution is entering the evaporator. There are densified solution and evaporated steam on the evaporator outlet. If the entire system is balanced using continuity equation, the balance of the densified components and enthalpy balance results in relationships 1 – 3.

$$m_0 - m_1 - m_2 = 0 \quad (1)$$

$$m_0\omega_0 - m_1\omega_1 = 0 \quad (2)$$

$$m_0h_0 - m_1h_1 - m_2h_2 + Q = 0 \quad (3)$$

Where:

m_0…Mass flow of the dilute solution flowing into evaporator [kg·h^{-1}],

m_1…Mass flow of densified solution at the evaporator outlet [kg·h^{-1}],

m_2…Evaporated steam mass flow [kg·h^{-1}],

h_0…Specific enthalpy of dilute solution flowing into evaporator [J·kg^{-1}],

h_1…Specific enthalpy of densified solution at the evaporator outlet [J·kg^{-1}],

h_2…Specific enthalpy of evaporated steam [J·kg^{-1}],

ω_0…Mass fraction of dilute solution flowing into evaporator [%],

ω_1…Mass fraction of densified solution at the evaporator outlet [%],,

ω_i…Mass fractions corresponding to the densified component [%],

Q…Heat [J·h^{-1}].

Value of the specific enthalpy h_2 corresponds to the amount of specific enthalpy of evaporated steam, i.e. specific enthalpy of saturated water vapor corresponding to the pressure in the evaporator. We consider mass and enthalpy balance of the evaporator for a dilute solution on the evaporator inlet of V_0=6 m^3·h^{-1}. The composition of the input dilute solution is given in table 1, specific density ρ_0=1200 kg·m^{-3} at temperature of 54 °C. The mass flow of solution at the inlet is:

$$m_0 = V_0\rho_0 = 6 \cdot 1200 = 7200\ kg \cdot h^{-1} \quad (4)$$

By applying the balance of component (2) we calculate mass flow of the solution at the outlet of evaporator m_1. If we use mass fraction values from table 1, we get:

$$m_1 = m_0 \frac{\omega_0}{\omega_1} = 7200 \frac{0{,}2508}{0{,}3569} = 5059{,}6\ kg \cdot h^{-1} \quad (5)$$

With help of the continuity equation (1) we can calculate evaporated steam mass flow, i.e. the required amount of evaporated water from the densified solution:

$$m_2 = m_0 - m_1 = 7200 - 5059{,}6 = 2140{,}4\ kg \cdot h^{-1} \quad (6)$$

Required heating output Q, which needs to be supplied to the evaporator can be expressed using the enthalpy balance (3):

$$Q = -m_0 h_0 + m_1 h_1 + m_2 h_2 = \frac{1}{3600}(-7200 \cdot 193443 + 5059{,}6 \cdot 384606 + 2140{,}4 \cdot 2682805 = 1748732\ W = 1749\ kW \quad (7)$$

Where the specific enthalpy values are taken from the database of Lauterbach Verfahrenstechnik GmbH, specifically from the source of thermophysical and transport properties of an aqueous solution of sulfuric acid with a composition corresponding to mass fraction of 18.7 % and value of enthalpy of saturated water vapor at pressure in the evaporator p_2 = 119325 Pa. Calculated values are summarized in the following text, which was calculated using MATLAB ® simulation system environment. [51]

- Inlet temperature: 54.0 °C
- Inlet volume flow: 6.00 $m^3 \cdot h^{-1}$
- Inlet mass flow: 7.20 $t \cdot h^{-1}$ (for 1200.0 $kg \cdot m^{-3}$)
- Inlet mass fraction: 0.251
- Outlet mass flow: 5.06 $t \cdot h^{-1}$
- Outlet mass fraction: 0.357 (required)
- Evaporated steam volume flow: 2.24 $m^3 \cdot h^{-1}$
- Evaporated steam mass flow: 2.14 $t \cdot h^{-1}$
- Heat exchanger specific power: 1749 kW
- Steam mass flow: 2.9 $t \cdot h^{-1}$ (130 °C, 2.70 bar)
- Boiling point: 108 °C (=104.6 + 3.4)
- Inner pipe diameter: 25.0 mm
- Outer pipe diameter: 37.0 mm
- Pipe length: 3834.0 mm
- Inner heat exchange surface: 84.3141 m^2
- Outer heat exchange surface: 124.7848 m^2
- Flow cross section: 0.1374 m^2
- Steam temperature: 130 °C
- Temperature difference: 22 °C
- Heat transfer coefficient (on the inner surface): 944 $W \cdot m^{-2} K^{-1}$
- Flow rate (inlet volume flow): 0.012 $m \cdot s^{-1}$

Heat transfer coefficient is related to the internal heat transfer area of heat exchanger. Temperature difference is corresponding to temperature of the condensing saturated steam and boiling point of the solution in the evaporator. The calculation is based on use of mass and enthalpy balance and it shows a relatively large difference between the amount of steam predicted by the calculation, i.e. 2.90 t·h-1, and the actual measured value, i.e. 2.40 t·h-1. This difference may be an inaccuracy in the chosen definition of the mass fraction of solutes in the densified solution. If we adjust the mass fraction to correspond to the heating steam consumption for a given operating state, we obtain following parameters. As can be seen, the mass fraction differs by approximately 3 %, which is not a very big difference. The mass fraction of dissolved substances was calculated based on the specific density of the resulting sample from chemical analysis, where the mass concentration of dissolved substances is determined. [9]

- Inlet temperature: 54.0 °C
- Inlet volume flow: 6.00 $m^3 \cdot h^{-1}$
- Inlet mass flow: 7.20 $t \cdot h^{-1}$ (for 1200.0 $kg \cdot m^{-3}$)
- Inlet mass fraction: 0.251
- Outlet mass flow: 5.53 $t \cdot h^{-1}$
- Outlet mass fraction: 0.327 (required)
- Evaporated steam volume flow: 1.75 $m^3 \cdot h^{-1}$
- Evaporated steam mass flow: 1.67 $t \cdot h^{-1}$
- Heat exchanger specific power: 1448 kW
- Steam mass flow: 2.4 $t \cdot h^{-1}$ (130 °C, 2.70 bar)
- Boiling point: 108 °C (=104.6 + 3.4)
- Inner pipe diameter: 25.0 mm
- Outer pipe diameter: 37.0 mm
- Pipe length: 3834.0 mm

- Inner heat exchange surface: 84.3141 m^2
- Outer heat exchange surface: 124.7848 m^2
- Flow cross section: 0.1374 m^2
- Steam temperature: 130 °C
- Temperature difference: 22 °C
- Heat transfer coefficient (on the inner surface): 781 $W \cdot m^{-2} K^{-1}$
- Flow rate (inlet volume flow): 0.012 $m \cdot s^{-1}$

9 Operational data processing

Given this is a technologically relatively complex process with many variables, for the purpose of this article the composition of diluted inlet solution has been established according to table 1. With a specific density of 1200 $kg \cdot m^{-3}$, the composition consists of 80 $g \cdot l^{-1}$ sulfuric acid H_2SO_4, 160 $g \cdot l^{-1}$ sodium sulfate Na_2SO_4 and 61 $g \cdot l^{-1}$ zinc sulfate $ZnSO_4$. The amount of heating steam that needs to be supplied to achieve the desired concentration of the spinning bath depends on the amount of inlet dilute solution. Since this is a variable value, measurements of operating conditions were performed for individual volumetric flow rates of the dilute solution on the inlet V_0. The histogram in graph 1 shows that most operating states concerning flow rates to quantify an interval 2 to 7 $m^3 \cdot h^{-1}$.

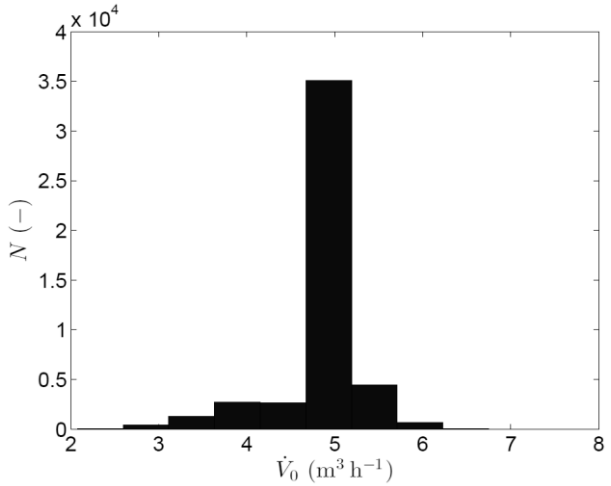

Graph 1 *Operating states according to volumetric flow rate of the dilute solution at the evaporator inlet*

Operating states however are not only classified according to flow rate but also are divided into 10 equal time groups. This basically means that time period during measurements took place, i.e. one complete operating cycle of the heat exchanger, was divided into 10 time groups. Each time group represents approximately 3 days of data acquisition. Acquired data in each time group has been processed through arithmetic mean algorithm. Data obtained are used to understand the evaporator behavior. In particular, comparing data in individual time groups could provide an answer to the unfavorable development of fouling due to process parameters progression.

An analysis of a boiling point increase of the solution is performed on a set of operational data as well. It represents the solution temperature measurements output. The boiling point of the solution depends on the absolute pressure in the evaporator, which can only approximately be determined. After calculating the absolute pressure and finding the boiling point of pure water, it is possible to determine the desired boiling point elevation ΔT_{fch} thanks to equation 8, using difference between temperature readings obtained by TI302 instrument and the saturation temperature: [9]

$$T = T_{sat} + \Delta T_{fch} \tag{8}$$

Where:
T…Boiling point of the solution [°C],
T_{sat}…Saturated steam temperature [°C],
ΔT_{fch}…Boiling point elevation [°C].

10 Measurements

As described in the previous chapter, there are several instruments and regulation in the technology, and data are being recorded and stored in SCADA master system. In the table 2 can be found a small part of continuous process data set for illustration. The actual measurement set of evaporator operating conditions contains tens thousands of records.

A development of selected operating parameters of the spinning bath evaporator over a complete operating cycle of approximately 30 days can be viewed on graph 2. The plot consider all inflow intervals of the dilute solution. The horizontal axis expresses real operating time in days, which allows direct interpretation of process behavior in relation to fouling progression. The plotted variables include the volumetric flow rate of the dilute solution at the evaporator inlet, the mass flow rate of heating steam, the temperature of the incoming steam, and the temperature of the solution inside the evaporator. Each variable is complemented by its corresponding linear regression trend, which enables identification of long-term tendencies within the operating cycle.

Tab. 2 *Part of the continuous process measurement data set*

	Flowmeter FIC314	Thermometer TIC318	Manometer PI207	Manometer PICAH312	Thermometer TI302	Flowmeter FIC301
[s^{-1}]	[$t \cdot h^{-1}$]	[°C]	[bar]	[bar]	[°C]	[$m^3 \cdot h^{-1}$]
04:53:00	1.957	128.01	1.7326	0.1840	105.73	4.978
04:54:00	1.845	128.01	1.7292	0.1849	105.73	4.944
04:55:00	1.959	128.01	1.7141	0.1892	105.90	5.030
04:56:00	1.989	128.24	1.7315	0.1837	106.02	4.891
04:57:00	1.993	128.18	1.7292	0.1814	106.02	4.944
04:58:00	2.054	128.13	1.7442	0.1765	105.96	4.974
04:59:00	1.926	127.89	1.7326	0.1707	106.02	4.891
05:00:00	1.833	127.60	1.7315	0.1681	105.96	4.887
05:01:00	1.987	127.66	1.7083	0.1780	105.90	4.857
05:02:00	1.934	128.01	1.7245	0.1852	105.84	4.978
05:03:00	1.959	128.13	1.7303	0.1866	105.84	4.948
05:04:00	1.942	128.01	1.7292	0.1884	105.84	4.978
05:05:00	1.845	127.95	1.7188	0.1829	105.96	4.826
05:06:00	1.977	128.01	1.7153	0.1814	105.96	5.061
05:07:00	2.025	128.13	1.7269	0.1800	106.02	4.865
05:08:00	1.908	127.95	1.7477	0.1771	106.02	4.913
05:09:00	1.969	127.66	1.7442	0.1722	106.02	5.273

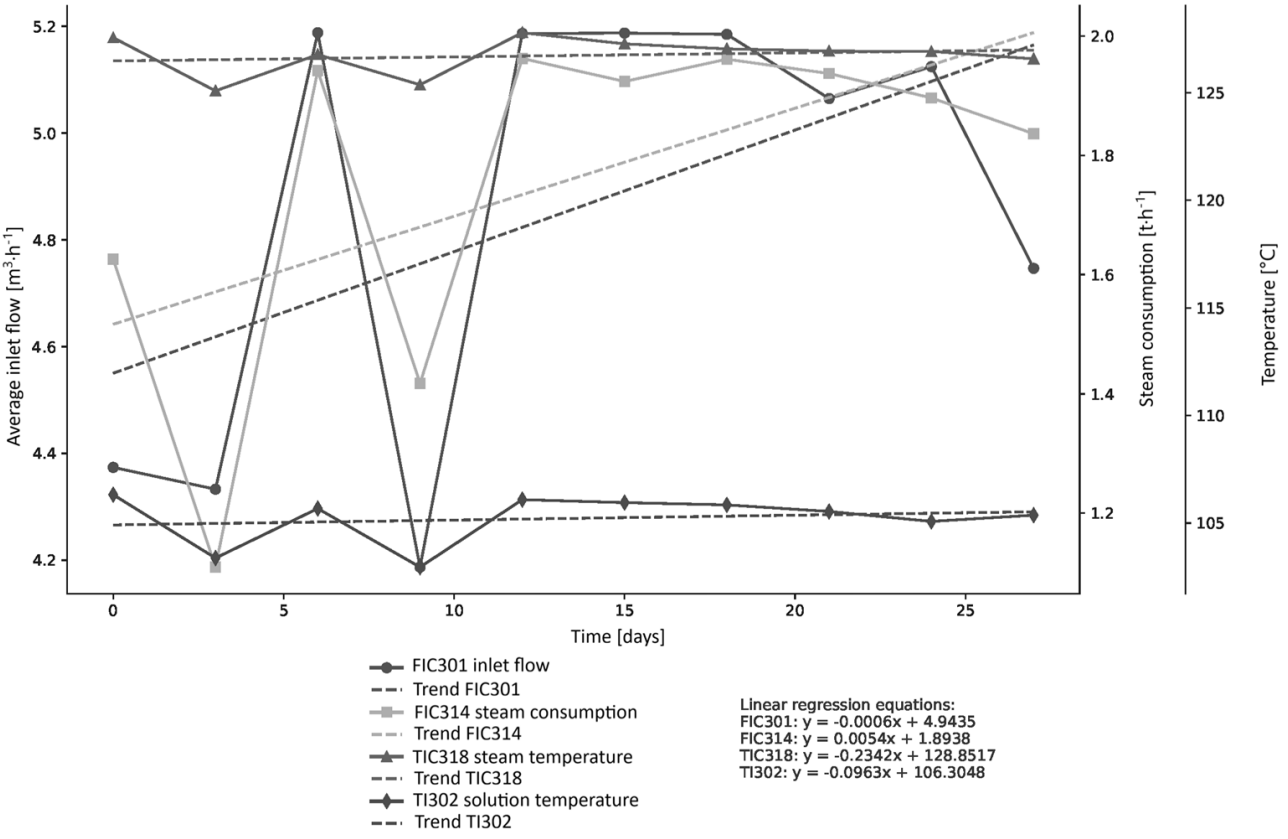

Graph 2 *Evaporator operation across all inflow intervals*

From the diagram it is evident that the volumetric flow rate of the dilute solution exhibits noticeable fluctuations throughout the cycle, which correspond to variations in operating conditions and production requirements. Despite these fluctuations, the regression trend indicates a slight increasing tendency over time. A similar behavior can be observed for the steam consumption, where short-term variability is present; however, the overall trend suggests a moderate increase in energy input as the operating cycle progresses. This behavior can be interpreted as a compensatory mechanism for the gradual formation of fouling layers on the heat transfer surfaces, which reduce heat transfer efficiency and require higher thermal input to maintain the desired evaporation rate.

In contrast to flow-related parameters, both monitored temperatures demonstrate relatively stable behavior over the entire period. The temperature of the heating steam shows only a minimal increasing trend, while the temperature of the solution inside the evaporator remains nearly constant with a very slight upward tendency. This indicates that the control system of the evaporator maintains stable thermal conditions despite ongoing changes in fouling and process load. The ability to keep temperatures within a narrow range suggests that regulation is primarily achieved through adjustments in flow rates rather than significant changes in temperature levels.

A practical operational model was fitted for steam mass flow FIC314, because the empirical condition is observed that steam consumption depends mainly on feed inflow and that steam temperature must gradually rise during the cycle as fouling develops. The simple model therefore uses inflow FIC301 and steam temperature TIC318 as continuous predictors, while an extended version adds time-frame fixed effects to represent cycle drift.

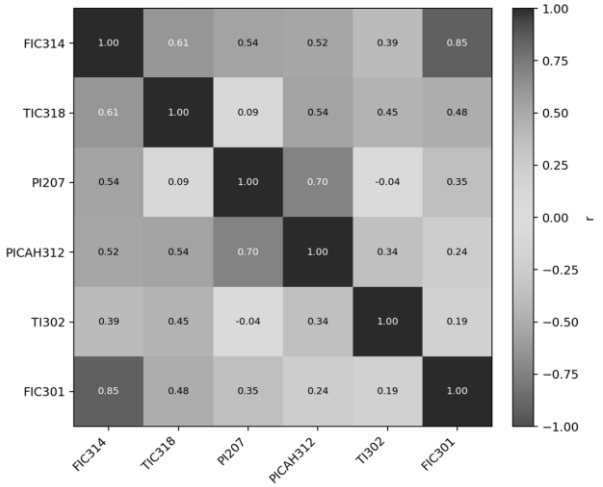

Graph 3 *Weighted Pearson correlation heatmap*

Simple Weighted Least Squares equation:

$$FIC314 = -4.9142 + 0.2872 \cdot FIC301 + 0.0425 \cdot TIC318 \quad (9)$$

The variable network is physically coherent: feed inflow drives steam demand, and steam/evaporator pressures move together. FIC301 is the dominant explanatory variable for FIC314; TIC318 provides an additional but smaller contribution. A compact operational model using only FIC301 and TIC318 already explains most of the variation in steam flow. Adding time-frame fixed effects substantially improves fit, which is consistent with slow operating-cycle drift and fouling effects.

Furthermore, dependence of volumetric flow rate of the inflowing dilute solution and steam consumption is correlated over time. As well as dependence of steam temperature and the solution temperature in the evaporator is observed. Monitoring took place at given intervals of the inflow of dilute solution to the evaporator, as described above. The trends of monitored quantities in the given interval are shown in graph 4. The left-hand side of the graph shows monitored dependences of volumetric flow rate of flowing dilute solution (green curve) on time and steam consumption (red curve) on time. The right-hand side of the graph shows dependences of steam temperature (blue curve) and temperature of the solution in the evaporator (yellow curve) on time. Labels in the graph indicate size of the interval. Number in parentheses indicate minimum and maximum amount of data in each time interval. For illustration graphs show measurements taken at intervals of 4.375, 4.875 and 5.5 $m^3 \cdot h^{-1}$ inflow of the dilute solution into the evaporator. From the trends it is clear, that steam consumption is almost constant throughout the heat exchanger's operating cycle, even though the volumetric flow rate of the solution increases during the operating cycle. Also, it can be seen that temperature of the steam as well as temperature of the solution in the evaporator is nearly constant throughout the entire operating cycle.

An analysis of boiling point elevation of the solution has been performed on the operational data set. These are the results of temperature measurements using TI302 thermometer. The temperature express boiling point of the solution at overpressure measured by PICAH312 pressure measurement. Based on the measurement of the boiling point increase of the spinning bath solution, the actual boiling point elevation has been determined as 3.4 °C. The graph shows decreasing tendency of the boiling point elevation, which may indicate changes in the concentration of the solution. [9]

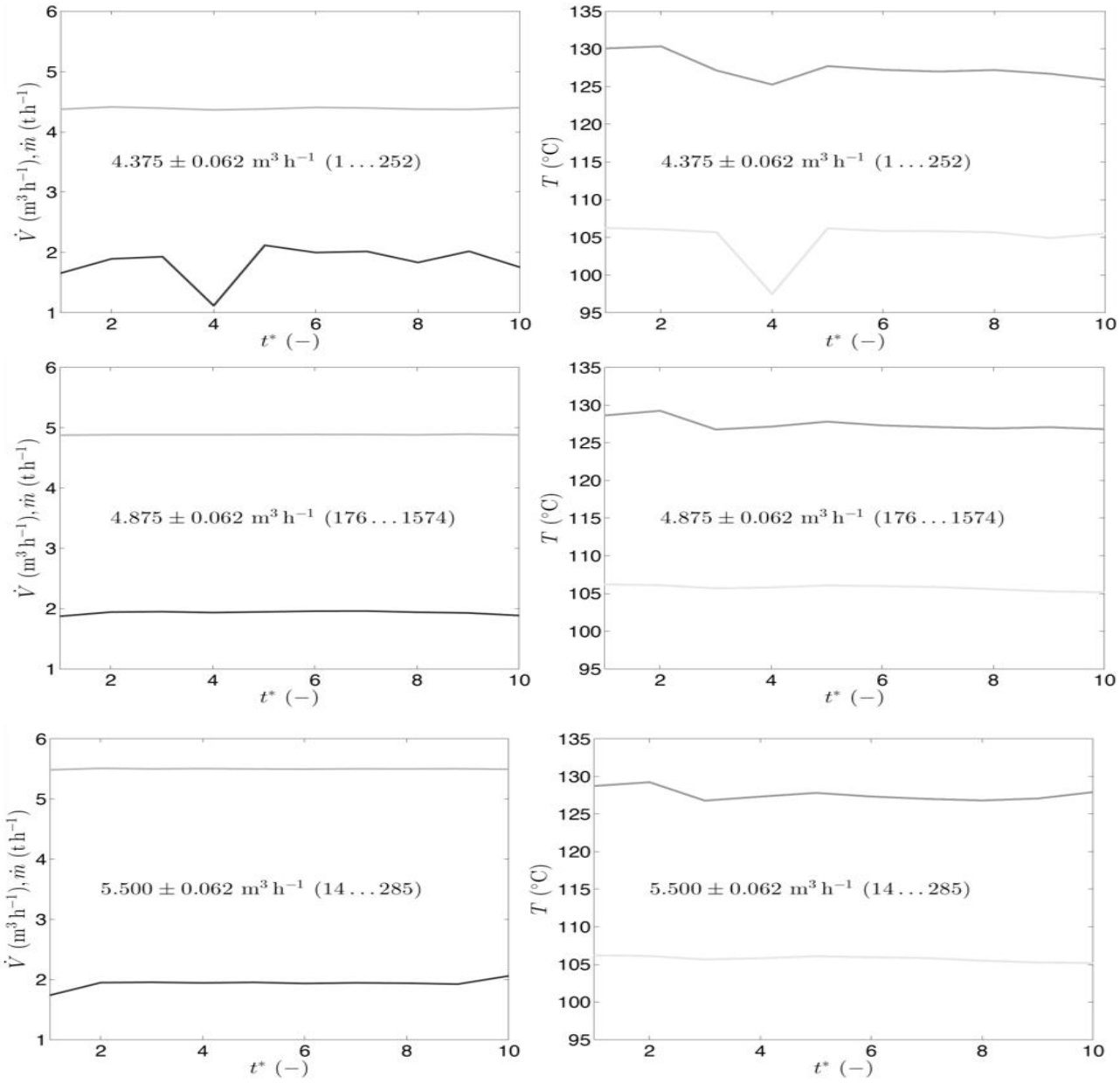

Graph 4 *Dependence of steam consumption, steam temperature and volumetric flow rate, temperature of dilute solution on time [9]*

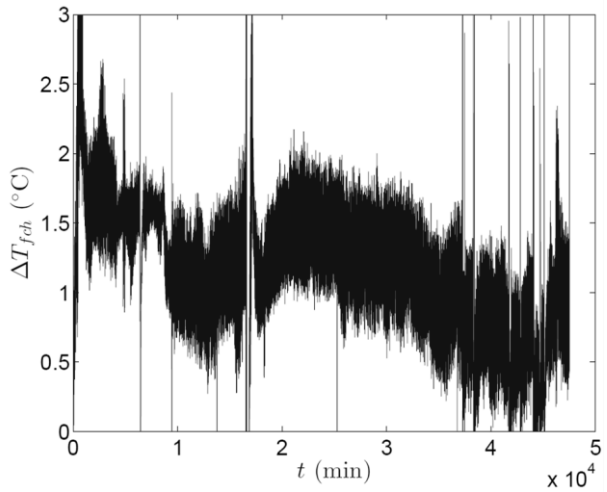

Graph 5 *Progress of the boiling point elevation during an operating period of the heat exchanger [9]*

11 Simulation

First simulation has been performed on heat exchanger, or rather one of its tubes. Since MATLAB ® calculates behavior along one tube of a heat exchanger which has geometric and process parameters corresponding to a real one, it was assumed ten times the inflow of dilute solution to the evaporator flowing through the heat exchanger. Also, it is assumed that heat exchanger tubes are clean, i.e. without deposits. Another prerequisite is the choice of a liquid model, for which an aqueous solution of sulfuric acid with a mass fraction of 18.7 % is selected. Whose boiling point elevation coincides with the actual solution, namely 3.4 °C.

- Inner pipe diameter: 25.0 mm
- Outer pipe diameter: 37.0 mm

- Pipe length: 3834.0 mm
- Pipe entry below surface: 4846.0 mm
- Number of pipes: 280
- Inner heat exchange surface: 84.3141 m²
- Outer heat exchange surface: 124.7848 m²
- Flow cross section: 0.1374 m²
- Fouling factor: 0.00000 m²kW^{-1}
- Mass flow: 20.00 kgs^{-1}
- Mean velocity in the pipe: 0.11 ms^{-1}
- Heat exchanger specific power: 3400 kW
- Absolute pressure: 1.193 bar
- Steam temperature: 130.0 °C (2.7 bar)
- Boiling point/surface: 108.0 °C (=104.6 + 3.4)

From the simulation results it can be stated that evaporator output in state of clean internal heat exchange surface, i.e. heat exchanger without any deposits, the heat exchanger specific power does exceed required specific power as per enthalpy balance. Following simulation illustrated condition where there is already 0.1 mm thick fouling layer that has formed on the inner surface of the heat exchange surface in the heat exchanger. Assuming thermal conductivity coefficient of 0.5 W·m-1K-1 the fouling factor is:

$$\frac{0{,}0001}{0{,}5} = 0{,}0002\ m^2KW^{-1} \qquad (10)$$

Based on that, as can be seen from the calculation, the heat exchanger performance would decrease by 40 %.

- Fouling factor: 0.00020 m²kW^{-1}
- Mass flow: 20.00 kgs^{-1}
- Mean velocity in the pipe: 0.11 ms^{-1}
- Heat exchanger specific power: 3400 kW
- Absolute pressure: 1.193 bar
- Steam temperature: 130.0 °C (2.7 bar)
- Boiling point/surface: 108.0 °C (=104.6 + 3.4)

The following graph 6 graphically shows development of some monitored quantities such as solution temperature in a pipe T_B, heat transfer coefficient of the condensing steam α_C, heat transfer coefficient of the densified solution flowing through a pipe α_B, steam quality x and specific enthalpy of solution flowing through a pipe h_B. The graph shows development of quantities where firstly the solution is heated to a boiling temperature, and then accompanied by convective boiling steam is being formed.

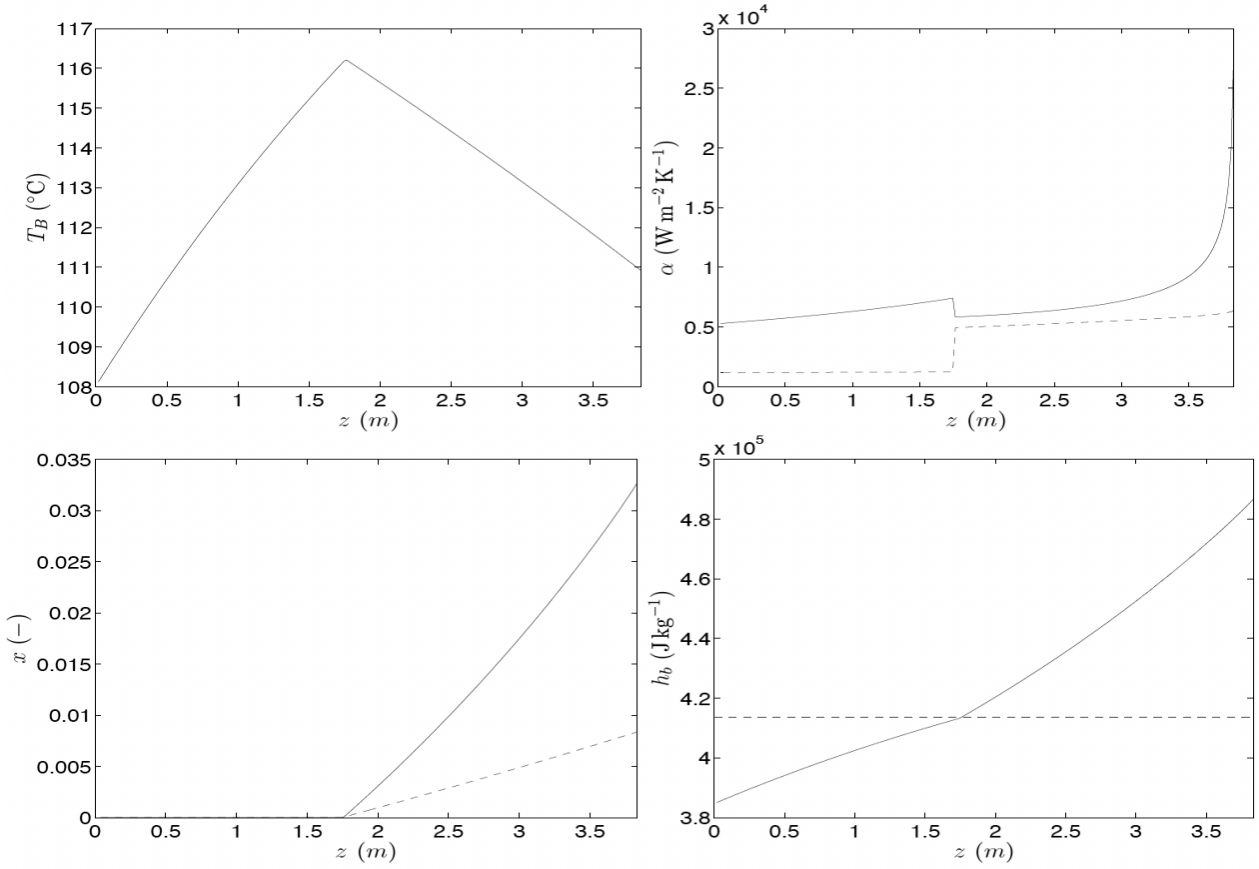

Graph 6 *Development of simulated quantities along the heat exchanger tube [9]*

In the graph showing development of heat transfer coefficient along heat exchanger tube, solid line represents heat transfer coefficient during condensation and dashed line represents heat transfer coefficient during boil. Section showing development of specific enthalpy of the solution, horizontal dashed line shows value of specific enthalpy at saturation limit, i.e. specific enthalpy of the solution corresponding to the onset of boil. With further growth of deposit layer characterized by a fouling factor of 0.001 m^2KW^{-1}, heat exchanger performance drops below the performance required for evaporation of the required amount of water from the dilute solution based on the enthalpy balance.

- Fouling factor: 0.00100 m^2kW^{-1}
- Mass flow: 20.00 kgs^{-1}
- Mean velocity in the pipe: 0.12 ms^{-1}
- Heat exchanger specific power: 889 kW
- Absolute pressure: 1.193 bar
- Steam temperature: 130.0 °C (2.7 bar)
- Boiling point/surface: 108.0 °C (=104.6 + 3.4)

The thermal resistance of deposits can then be compensated by increased parameters of the heating steam properties, i.e. by increasing the steam temperature up to 140.2 °C at 3.6 bar.

- Fouling factor: 0.00100 m^2kW^{-1}
- Mass flow: 20.00 kgs^{-1}
- Mean velocity in the pipe: 0.12 ms^{-1}
- Heat exchanger specific power: 1446 kW
- Absolute pressure: 1.193 bar
- Steam temperature: 140.2 °C (3.6 bar)
- Boiling point/surface: 108.0 °C (=104.6 + 3.4)

While maintaining temperature of the heating steam, the same heat exchanger performance can be achieved by increasing flow rate of the solution through the heat exchanger. If we increase the flow rate through the heat exchanger to a value corresponding 140 times the inflow of dilute solution to evaporator, we can achieve the same performance. In this case, however, the solution would practically not evaporate, rather than heated up only. The mass flow rate of the solution would have to be 280 $kg·s^{-1}$ and throughput would have to be achieved by additional circulation pump. The favorable flow rate velocity 1.6 $m·s^{-1}$ could have a positive effect on limiting rate of fouling formation. [9]

- Fouling factor: 0.00100 m^2kW^{-1}
- Mass flow: 280.00 kgs^{-1}
- Mean velocity in the pipe: 1.62 ms^{-1}
- Heat exchanger specific power: 1448 kW
- Absolute pressure: 1.193 bar
- Steam temperature: 130.0 °C (2.7 bar)
- Boiling point/surface: 108.0 °C (=104.6 + 3.4)

12 Assessment for forced circulation

Governing basis for the preliminary recommendation it quantifies the order of magnitude required for recirculation if the conversion is intended to preserve duty while limiting the need to raise steam temperature and pressure. Accordingly, recommendation adopts 280 $kg·s^{-1}$ as the primary design basis for the circulation loop, while still treating the resulting pump head as preliminary because full piping isometric or a verified list of local hydraulic resistances is not yet clearly defined. For the reconciled operating case overall evaporator duty does not disappear when a circulation pump is introduced. What changes is the recirculating mass flow through the exchanger and thus the exchanger-side temperature approach, boiling pattern, internal heat-transfer coefficient, and propensity to foul.

To make the circulation duty explicit, it is convenient to define a circulation ratio R as the ratio between recirculating mass flow m_{circ} and fresh-feed mass flow m_f:

$$R = \frac{m_{circ}}{m_f} \tag{11}$$

With m_f = 7.20 $t·h^{-1}$ = 2.00 $kg·s^{-1}$ and the source-derived forced-circulation requirement m_{circ} = 280 $kg·s^{-1}$, the implied circulation ratio is approximately 140. This is high but not implausible for a scaling service where the design intent is to keep most of the liquor in liquid phase while exposing only a small fraction of each pass to actual evaporation. In other words, the exchanger becomes primarily a heater and circulation device, while vapor disengagement remains concentrated in the evaporator vessel. The practical implication is that the exchanger no longer needs to generate a large vapour fraction inside the tubes to sustain circulation. Instead, it needs to transfer enough sensible and incipient-boiling energy to a very large recirculating liquid stream so that the bulk evaporator can maintain the required overall mass evaporation rate.

The source simulation indicates that under the forced-flow case the average tube velocity reaches roughly 1.62 $m·s^{-1}$. This is consistent with the volumetric flow implied by the 280 $kg·s^{-1}$ recirculation rate. Assuming an average circulating-liquor density ρ_{circ} near 1300 $kg·m^{-3}$, the volumetric rate becomes.

$$Q_{circ} = \frac{m_{circ}}{\rho_{circ}} = \frac{280}{1300} = 0.215\ m^3 \cdot s^{-1} = \ 774\ m^3 \cdot h^{-1} \tag{12}$$

And the mean tube velocity is:

$$v = \frac{Q_{circ}}{A} = \frac{0.215}{0.1374} \approx 1.57\ m \cdot s^{-1} \tag{13}$$

That agrees satisfactorily with the source value of approximately 1.62 m·s^{-1} once rounding and density variation are acknowledged. This confirms that the source-based recirculation requirement and the exchanger geometry are mutually consistent. Therefore, for preliminary sizing purposes, the pump should be based on a rated volumetric flow of about 775 m^3·h^{-1} at normal concentration, with an allowance to 800 m^3·h^{-1} for control margin and viscosity uncertainty.

The key missing element is not the circulation flow but the loop pressure drop. The pump head must therefore be estimated from the exchanger tubes, the connecting nozzles and piping, the vessel entry and exit losses, control fittings, and a reasonable fouling margin. Because the loop is essentially recirculating between the evaporator body and the external exchanger, static head does not dominate unless the suction conditions are poor or the nozzle elevations create persistent differential liquid levels. In most forced-circulation evaporators the required pump head is governed mainly by dynamic losses. This is advantageous because dynamic losses can be estimated with transparent equations and then expanded by prudent margin.

The basic friction loss in the exchanger tubes may be estimated by the Darcy-Weisbach equation, written here in head form as:

$$H_f = f(\frac{L}{D}) \cdot (\frac{v^2}{2g}) \tag{14}$$

Or in pressure form as:

$$\Delta p_f = f(\frac{L}{D}) \cdot (\frac{\rho v^2}{2}) \tag{15}$$

Where:
f…The Darcy friction factor,
L…The effective tube length,
D…The hydraulic diameter,
v…The mean velocity,
g…Gravitational acceleration,
ρ…Liquid density.

For a preliminary calculation one may take L = 3.834 m, D = 0.025 m, v ≈ 1.57 to 1.62 m·s^{-1}, and ϱ ≈ 1300 kg·m^{-3}. The exact friction factor depends on Reynolds number, viscosity, and relative roughness. However, because the solution is hot, water-rich, and moving in relatively smooth graphite tubes, a provisional Darcy factor around 0.03 is a defensible first estimate for engineering screening. Substituting these values gives a straight-tube pressure drop on the order of only several kilopascals. Using v = 1.62 m·s^{-1}, for example, yields.

$$\Delta p_f = 0.03 \cdot (\frac{3.834}{0.025}) \cdot (\frac{1300 \cdot 1.62^2}{2}) \approx 8\ kPa \tag{16}$$

This result is deliberately simple and should not be overstated. It indicates that the long straight tubes alone are not likely to dictate a very high pump head. The more significant losses are expected in the tube-sheet entries and exits, manifolding into exchanger sections, return nozzles, vessel connections, bends, reducers, isolation valves, and any flow-control element added for balancing or turndown. Those contributions can be collected by a local-loss coefficient sum ΣK, giving:

$$\Delta p_{local} = \sum K\ (\frac{\rho v^2}{2}) \tag{17}$$

If a moderate equivalent local-loss coefficient of about 10 to 15 is assumed for the complete circulation loop, the corresponding local pressure drop at the same velocity is roughly 17 to 25 kPa. When added to the straight-tube contribution, the total clean-loop drop becomes on the order of 25 to 35 kPa, corresponding to about 2 to 3 m of liquid head. On its own, that would suggest a very small pump head. Yet using that value directly for equipment selection would be unsafe because the exchanger is known to foul, the real liquor viscosity may exceed the water-like assumption, plant piping details are incomplete, and the final design should include control and ageing margin. For this reason, it is appropriate to elevate the design head beyond the clean calculated minimum.

A prudent preliminary design envelope is therefore to select a pump for 775 to 800 m^3·h^{-1} at 8 to 12 m differential head. The lower part of that range is already generous relative to the likely clean hydraulic requirement, while the upper part gives room for ageing, unforeseen nozzle losses, line roughness, limited throttling, future flow optimisation, and uncertainty in physical properties. The use of a variable-frequency drive is strongly recommended so that the operating point can be trimmed after commissioning.

The energy balance of the circulation pump must be treated separately from the evaporator enthalpy balance because the pump does not supply latent heat for evaporation in the same sense as the heating steam. Instead, it adds mechanical energy to the recirculating liquid, which is mostly dissipated as hydraulic pressure rise and ultimately as heat through friction. In a steady circulation loop, the pump energy balance can be written for an incompressible liquid as:

$$p_h = \rho \cdot g \cdot Q \cdot H \tag{18}$$

Where:

P_h…The hydraulic power transferred to the liquid,

ρ…Density,

Q…Volumetric flow,

H…Total developed head.

The shaft power requirement of the pump is then:

$$p_{shaft} = \frac{p_h}{\eta_p} \tag{19}$$

And the electrical power drawn at the motor terminals is:

$$p_{el} = \frac{p_h}{(\eta_p \cdot \eta_m \cdot \eta_{VFD})} \tag{20}$$

Where:

ηp…Pump hydraulic efficiency,

ηm…Motor efficiency,

ηVFD…Variable-frequency-drive efficiency if a VFD is installed.

The liquid-side energy gain per unit mass can also be expressed as:

$$e_p = g \cdot H \tag{21}$$

So that the incremental enthalpy rise due to pumping, if entirely dissipated into the liquid, is approximately:

$$\Delta h_p \approx g \cdot H \tag{22}$$

For a head of 10 m, this gives $\Delta h_p \approx 98$ J·kg^{-1}, which is negligible compared with the thousands of kilojoules per kilogram associated with latent heat of evaporation. This confirms that the pump is not a thermal substitute for steam; it is a hydraulic enabler whose benefit appears through better heat transfer and reduced fouling rather than through direct thermal contribution.

Using the preliminary design flow Q = 800 m^3·h^{-1} = 0.222 m^3·s^{-1}, density ρ = 1300 kg·m^{-3}, head H = 10 m, pump efficiency η_p = 0.75, motor efficiency η_m = 0.95, and VFD efficiency η_{VFD} = 0.97, the power becomes:

$$p_H = 1300 \cdot 9.81 \cdot 0.222 \cdot 10 \approx 28.3\ kW \tag{23}$$

$$p_{shaft} = \frac{28.3}{0.75} \approx 37.7\ kW \tag{24}$$

$$p_{el} = \frac{28.3}{(0.75 \cdot 0.95 \cdot 0.97)} = 40.1\ kW \tag{25}$$

These values justify recommending a 55 kW installed motor because the absorbed power at the selected point is likely around 40 kW, while the larger motor rating gives allowance for viscosity excursions, off-design operation, modest head increase, and future process optimisation.

13 Technical-economic comparison

A sound preliminary CAPEX model for the forced-feed conversion should include at least the circulation pump, motor and drive, suction and discharge piping modifications, nozzles and supports, isolation valves, any recirculation control valve or bypass, instrumentation, electrical works, structural steel, installation labour, and commissioning.

A common conceptual-cost approach is to scale equipment purchase cost from a reference size using the capacity-factor relationship:

$$C_P = C_{ref} \frac{S}{S_{ref}}^{n \cdot F_M \cdot F_T \cdot F_P} \tag{26}$$

Where:

C_p…The estimated purchased cost of the pump package,

C_{ref}…The cost of a known reference item,

S…The selected size parameter,

S_{ref}…The reference size parameter,

n…The cost-scaling exponent,

F_M, F_T, and F_P…Correction factors for material, temperature/corrosion service, and pressure or special design features.

For pumps, S may be represented by absorbed power, by a hydraulic size index involving flow and head, or simply by vendor quotation interpolation. The important point is that the installation environment indicates a severe corrosive and scaling chemical environment; therefore, the material factor cannot be ignored. Carbon steel would likely be inappropriate for direct wetted service unless reliably protected, and the package should be priced with suitable corrosion-resistant wetted materials, linings, or a chemically isolated hydraulic design.

Once the purchased-equipment cost is estimated, the installed cost may be expressed by a bare-module or installation-factor method, for example:

$$C_{installation} = C_p \cdot F_{BM} \tag{27}$$

Operating cost must be evaluated more broadly than pump electricity alone. In fact, the most important economic effect of the forced-circulation conversion may not be energy use but avoided losses caused by fouling, cleaning, exchanger switching, steam escalation, and production interruption. The total annual operating-cost impact of the modification can therefore be expressed as a difference between the new and existing regimes:

$$\Delta C_{OPEX} = C_{el.pump} + C_{maint.pump} + C_{spare\ parts} + C_{extra\ aux.} - (C_{clean.saved} + C_{downtime\ saved} + C_{steam\ saved} + C_{damage\ saved}) \quad (28)$$

Where a negative value indicates net annual savings. The first direct term is the electrical-energy cost of the circulation pump. Using the electrical power derived above, annual running time t_{op}, and unit electricity price C_{el}, one obtains:

$$C_{el.pump} = p_{el} \cdot t_{op} \cdot C_{el} \quad (29)$$

If the pump draws around 40 kW and runs 8000 $h \cdot a^{-1}$, the annual electricity consumption is about 320 $MWh \cdot a^{-1}$. The monetary value then depends on the site electricity tariff. Because tariffs vary substantially in time and contract, it is more rigorous to leave the cost equation symbolic. Even so, the energy number itself is useful: it shows that the electrical duty is industrially significant but not extraordinary.

Pump maintenance cost may be estimated as a fraction of installed pump-package cost or through an activity-based model. A simple early-stage equation is:

$$C_{maint.pump} = f_{maint.} \cdot C_{pump\ package} \quad (30)$$

Where $f_{maint.}$ may reflect routine inspections, seal replacements, bearing replacements, lubrication, alignment, and overhauls. In critical corrosive service, it is wise to include spare mechanical seals, bearings, and one rotating assembly or impeller if lead times are long. This is particularly relevant because a forced-circulation pump becomes mission-critical unless a standby unit is installed.

Against these additional costs one must credit the savings expected from a lower fouling rate. If forced circulation extends this interval, even by a factor of two rather than an order of magnitude, the effect on maintenance labour and exchanger availability may be substantial. Cleaning-cost savings may be represented as:

$$C_{clean.saved} = (N_{clean\ old} - N_{clean\ new}) \cdot \frac{C_{clean}}{event} \quad (31)$$

Downtime savings can be written similarly as:

$$C_{downtime\ saved} = (t_{down\ old} - t_{down\ new}) \cdot C_{lost\ production} \quad (32)$$

Which is often the dominant economic term in continuous-process industries. The structure of the equation for downtime should nevertheless be included because it is often the decisive term in retrofit justification. If exchanger cleaning currently forces throughput reduction, equipment changeover, or unstable operation in the downstream spinning-bath preparation chain, the economic penalty may easily exceed the cost of pump electricity.

Steam-cost savings can also be formulated, though they should be treated cautiously. If forced circulation maintains the required 1448 kW duty at about 130 °C steam instead of requiring higher steam conditions, then some fuel or utility savings may result. The annual steam-cost difference may be written as:

$$C_{steam\ saved} = (m_{steam\ old} \cdot h_{steam\ old} - m_{steam\ new} \cdot h_{steam\ new}) \cdot t_{op} \cdot C_{steam\ eq.} \quad (33)$$

The stronger economic case rests on exchanger availability, less aggressive steam escalation, fewer maintenance interventions, and reduced collateral damage to coatings and structural parts.

To combine capital and operating effects in one annual criterion, the engineer may evaluate the equivalent annual cost of the retrofit as:

$$EAC = A_{cap} + C_{el.pump} + C_{maint.pump} + C_{spares} - C_{savings\ tot.} \quad (34)$$

Where $C_{savings\ tot.}$ includes all avoided cleaning, downtime, steam, and damage-related costs. If EAC is negative relative to the present arrangement, the retrofit is economically favourable. Even if it is slightly positive on direct cost alone, the project may still be justified when reliability, operability, and safety margins are strategically important.

14 Impact on the overal reliability

In the present natural-circulation system, the dominant operational problem is not random catastrophic fracture as the first event, but progressive performance degradation caused by deposit growth. That degradation then triggers secondary stresses:

operators raise steam pressure and temperature, the exchanger operates with increasing thermal resistance, eventual cleaning is required, and the repeated cycle of operation and maintenance exposes graphite tubes, coatings, gaskets, and welded joints to thermal and mechanical ageing.

Forced circulation changes this pattern in several beneficial ways. First, it raises the liquid-side velocity and should therefore reduce the net deposition rate, which attacks the dominant initiating mechanism. Second, by making circulation less dependent on buoyancy, it stabilises the exchanger-side hydraulic regime even when thermal conditions drift. Third, it should reduce the need to compensate fouling by escalating steam state, thereby reducing thermal stress on equipment. Fourth, if the cleaning interval is extended, the number of shutdowns, line openings, manual interventions, and coating-damaging maintenance actions should fall. These changes primarily improve availability and maintainability, though they may also improve intrinsic reliability by reducing exposure to stressors.

The countervailing effect is obvious: a circulation pump introduces bearings, seals, coupling or integrated drive elements, potential cavitation risk, and electrical/control dependencies. If only one pump is installed, the system may swap a slowly developing exchanger-fouling problem for a sudden single-point rotating-equipment failure. Therefore the dependability value of the conversion depends strongly on system architecture. A forced-circulation retrofit without standby capacity may improve thermal performance but still disappoint in availability. By contrast, a one-duty-one-standby arrangement with automatic changeover, permissive logic, and condition monitoring can convert the pump from a vulnerability into a manageable and redundant subsystem. This is precisely why IEC 60300-3-1 is useful: it reminds the analyst to choose a method appropriate not only to component failure rates but also to system structure, maintenance concept, and decision purpose.

The natural-circulation train crosses below the required 1448 kW at about 0.307 mm fouling thickness, which is about 18.4 days into a 30day cycle if deposit growth is treated as roughly linear. That means the train is functionally below required duty for about 38.6 % of the cycle unless steam is escalated or equipment is switched.

Using linear interpolation between the given fouled states:

$$R_{f,crit.} = R_{f,1} + \frac{Q_1 - Q_{req}}{Q_1 - Q_2}(R_{f,2} - R_{f,1}) = 0.0002 + \frac{2046 - 1448}{2046 - 889}(0.0010 - 0.0002) = 0.000613\ m^2KW^{-1} \quad (35)$$

The fouling conductivity is about 0.5 $Wm^{-1}K^{-1}$, so deposit thickness is:

$$\delta_{crit} = k \cdot R_{f,crit.} = 0{,}5 \cdot 0.000613 = 0.307\ mm \quad (36)$$

If the fouling layer grows approximately from 0 to 0.5 mm in 30 days, then critical time threshold is:

$$t_{crit.} = 30 \cdot \frac{0.307}{0.5} = 18.4\ days \quad (37)$$

So for the remaining 30-18.4=11.6 days the active train is below required duty. Approximating probability by fraction of cycle spent below required duty:

$$P_{U,base} = \frac{11.6}{30} = 0.386 \approx 38.6\ \% \quad (38)$$

So the current natural-circulation arrangement has an estimated 38.6% probability of functional unavailability over a monthly cycle, unless operators compensate by raising steam pressure/temperature or switching equipment. As documented as when duty falls from 1448 kW required to 889 kW available.

$$\Delta Q_{max} = 1448 - 889 = 559\ kW \quad (39)$$

Relative shortfall is:

$$\frac{559}{1448} = 0.386 \quad (40)$$

So the instantaneous consequence is about 38.6 % lost thermal capacity. Assume the shortfall rises roughly linearly from 0 to 559 kW during the last 11.6 days of the cycle. Average shortfall over that period is:

$$\Delta Q_{avg} = \frac{0 + 559}{2} = 279.5\ kW \quad (41)$$

Expected lost thermal service per month then:

$$E_{loss} = 279.5 \cdot 11.6 \cdot 24 = 77818\ kWh \approx 77.8\ MWh \quad (42)$$

So the current arrangement loses about 77.8 MWh per month of effective evaporation duty on this simplified basis.

With a pump introduced into the system a new failure mode needs to be assumed because pump failure statistics is not known.

- Assumed pump MTBF = 2 years = 17,520 h
- Assumed MTTR = 8 h

Time-based unavailability of a single pump is:

$$Q_{p1} = \frac{MTTR}{MTBF + MTTR} = \frac{8}{17520 + 8} = 4.56 \cdot 10^{-4} \approx 0.0456\% \quad (43)$$

If we consider installing a cold back up pump, then for a one out of two duty and standby pump pair, using the same single-pump unavailability and a modest 5 % common-cause factor:

$$Q_{p2} = \beta Q_p + (1 - \beta) Q_p^2 = 0.05 \cdot (4.56 \cdot 10^{-4}) + 0.95(4.56 \cdot 10^{-4})^2 = 2.30 \cdot 10^{-5} \approx 0.0023\% \quad (44)$$

From current system to the forced feed system with duty and stand by pump pair:

$$\Delta P_u = 38.6\% - 0.0023\% = 38.598\% \quad (45)$$

Relative probability reduction:

$$\frac{38.6 - 0.0023}{38.6} = 0.99994 \approx 99.994\% \quad (46)$$

If the two-pump system is available, the duty deficit from fouling is essentially removed:

$$\Delta Q_{p2} \approx 0\ kW \quad (47)$$

Expected lost duty due only to a pump-system unavailability, assuming full loss during the rare common-cause outage:

$$E_{loss} = 1448 \cdot 720 \cdot 2.30 \cdot 10^{-5} \approx 24\ kWh \cdot month^{-1} \approx 0.024\ MWh \cdot month^{-1} \quad (48)$$

If natural circulation remains available as degraded fallback, the consequence is even smaller. Relative consequence reduction:

$$\Delta E_{loss} = 77.8 - 0.024 = 77.776\ MWh \cdot month^{-1} \quad (49)$$

Relative consequence reduction:

$$\frac{77.8 - 0.024}{77.8} = 0.99969 \approx 99.97\% \quad (50)$$

If the enhancement concerns duty and standby pumps, auto changeover, condition monitoring, and preserved degraded fallback, it removes the dominant cause of unavailability described in the study: fouling-driven thermal collapse. The system then shifts from a high-probability progressive loss of function to a very low-probability equipment failure scenario.

15 Conclusion

Spinning bath evaporator analyses revealed that most operating states fall into flow rate interval between 2 to 7 $m^3 \cdot h^{-1}$. During evaporator operation a layer of glauberite salts deposits on the heat exchanger surface of heat exchangers. From the operational data measurements concerning one complete operation cycle of heat exchanger, its parameters such as steam temperature and pressure on the heat exchanger inlet, temperature and pressure in the evaporator, practically do not change. It can be concluded that evaporation of spinning bath solution nearly has a constant progression. Furthermore, it is established that:

- To process dilute solution with volume flow rate at 6 $m^3 \cdot h^{-1}$, an exchanger specific power of 1448 kW is required,
- Thermal conductivity coefficient of 0.495 $W \cdot m^{-1}K^{-1}$has been established.

The simulation determined that:

- In case of perfectly clean heat exchanger heat transfer surface, the heat exchanger power is equal to 3400 kW assuming ten times the amount of solution flowing through the heat exchanger into evaporator,
- A glauberite layer with a thickness of 0.1 mm corresponds to a fouling factor of 0.0002 m^2kW^{-1}, i.e. the heat exchanger output is 2046 kW,
- A glauberite layer with a thickness of 0,5 mm corresponds to a fouling factor of 0.001 m^2kW^{-1}, i.e. the heat exchanger output is 889 kW.

Given the measured values, it could mean that no fouling is formed during the evaporator's operation and it only begins to form after an „incubation "period, which coincides with the length of the standard heat exchanger operation cycle. Or perhaps evaporator output changes, so solution concentration may reduce on the evaporator outlet during the operating cycle of heat exchanger. Since the amount of evaporated water is not measured, it is not possible to verify the hypothesis other than by measuring the composition of the resulting solution during the entire operating cycle of the heat exchanger. Solution flow rate increase through heat exchanger would bring an increase in performance and probably would also extend time between cleanings. In this case, however, there is no model of deposit formation available and it would be necessary to determine the effect of flow velocity and temperature on the rate of deposit formation using a given solution and an experimental heat exchanger. [52] The circulation pump that would

be used in case of evaporator conversion to a forced circulation evaporator would have to ensure a volume flow rate of 800 $m^3 \cdot h^{-1}$; rated differential head 10 m; allowable operating window 700 to 850 $m^3 \cdot h^{-1}$; best-efficiency-point preference near 775 $m^3 \cdot h^{-1}$; liquid temperature 105 to 110 °C in normal service; liquid density 1200 to 1300 $kg \cdot m^{-3}$; corrosive sulfate-bearing liquor with anti-corrosion lining or alloy selection matched to the chemical environment; and NPSH verification required from the final suction arrangement.Given the requirements for the volume flow rate of the circulation pump, if a decision is made to use forced circulation, it would be appropriate to consider structural modifications to multi-pass heat exchanger. [9] The ratio of pump electrical power to required evaporator thermal duty is about 40 / 1448 ≈ 2.8 %, showing that the electricity penalty is comparatively small relative to the thermal service being protected. More importantly, if forced circulation successfully suppresses the severe fouling state that drives duty down to about 889 kW under fixed steam conditions, then the pump's electrical consumption is economically and operationally justified by the avoided loss of thermal performance and maintenance interruptions. Not every dependability-improving retrofit should be evaluated solely on energy consumption, especially when the existing system suffers from chronic performance collapse caused by a known physical mechanism.

Acknowledgement

Paper created on behalf of project „Ebner/I" Glanzstoff – Bohemia s.r.o., Terezínská 60, 410 02 Lovosice, Czech Republic and project CULS IGA: 2022:31190/3112/3109.

References

[1] R. L. SHILLINg, "Perry's chemical engineers' handbook. Section 11, Heat-transfer equipment," 2008, doi: 10.1036/0071511342.

[2] M. KALLISKI, B. VOGLAUER, G. SEYFRIEDSBERGER, C. JASCH, T. RÖDER, AND S. ENGELL, "Resource ficient operation of an evaporator network in the viscose fiber production," *Computer Aided Chemical Engineering*, vol. 40, pp. 1735–1740, Jan. 2017, doi: 10.1016/B978-0-444-63965-3.50291-9.

[3] Y. LI, J. PENG, X. LIU, D. SONG, W. XU, AND K. ZHU, "Dissolving waste viscose to spin

[4] B. N. JACKSON, "Vertical tube natural circulation evaporators," *Heat Recovery Steam Generator Technology*, pp. 65–80, Jan. 2017, doi: 10.1016/B978-0-08-101940-5.00004-X.

[5] Y. XIAO AND G. CUI, "A novel mass-heat exchange network analogy, regression, and synthesis method for mass exchanger networks," *Heliyon*, vol. 9, pp. 2405–8440, 2023, doi: 10.1016/j.heliyon.2023.e20574.

[6] J. DARAND AND A. JAFARIAN, "Long-term simulation of crystallization fouling in a forced circulation crystallizer," *Int. J. Heat Mass Transf.*, vol. 231, p. 125845, Oct. 2024, doi: 10.1016/J.IJHEATMASSTRANSFER.2024.125845.

[7] V. BOUR-BEUCLER, "Commissioning, operation cleaning and maintenance," *Corrosion Management of Seawater Cooling Systems*, pp. 145–162, Jan. 2024, doi: 10.1016/B978-0-443-15235-1.00009-3.

[8] E. CÉZOVÁ, "Economical and Statistical Optimization of the Maintenance in the Production Process," *Manufacturing Technology*, vol. 23, no. 1, pp. 32–39, 2023, doi: 10.21062/MFT.2023.004.

[9] DOSTÁL MARTIN, "Ebner/I," Praha, Aug. 2017.

[10] X. P. ZHOU, E. B. DU, AND Y. T. WANG, "Chemo-mechanical coupling bond-based peridynamic model for electrochemical corrosion and stress chemical corrosion," *Eng. Anal. Bound. Elem.*, vol. 151, pp. 360–369, Jun. 2023, doi: 10.1016/J.ENGANABOUND.2023.03.013.

[11] W. WANG *et al.*, "Continuous fibers featuring high phase change enthalpy fabricated by melt spinning for thermal management," 2024, doi: 10.1016/j.est.2024.113690.

[12] J.-P. SIMONIN, "Modeling of dilution enthalpies within implicit-solvent models for electrolytes," *J. Mol. Liq.*, vol. 394, p. 123801, 2024, doi: 10.1016/j.molliq.2023.123801.

[13] S. KARGAR, Z. BANIAMERIAN, AND J. L. MORAN, "Molecular dynamics calculations of the enthalpy of vaporization for different water models," *J. Mol. Liq.*, vol. 393, 2024, doi: 10.1016/j.molliq.2023.123455.

[14] F. MOKHTARI *et al.*, "Journal Pre-proofs Recent progress in electrospun polyvinylidene fluoride (PVDF)-based nano-fibers for sustainable energy and environmental applications Recent progress in electrospun polyvinylidene fluoride (PVDF)-based nanofibers for sustainable energy and environmental applications," 2024, doi: 10.1016/j.pmatsci.2024.101376.

[15] H. GUO, Z. ZHANG, AND Y. ZHU, "Study on the effect of stretching behavior on the properties of PVDF films and mechanism," *Polymer (Guildf).*, vol. 297, p. 126884, Mar. 2024, doi: 10.1016/J.POLYMER.2024.126884.

[16] R. L. SHILLING, "Perry's chemical engineers' handbook. Section 11, Heat-transfer equipment," 2008.

[17] J. VESELA, P. BENEŠ, AND D. BRICÍN, "Effect of Thermal Ageing on Changes in Modulus of Elasticity E Measured by Ultrasound, Bending Test and EBSD," *Manufacturing Technology*, vol. 25, no. 3, pp. 405–412, Jul. 2025, doi: 10.21062/MFT.2025.038.

[18] R. KAMAL KAUR, B. PANDEY, AND L. K. SINGH, "Dependability analysis of safety critical systems: Issues and challenges," *Ann. Nucl. Energy*, vol. 120, pp. 127–154, Oct. 2018, doi: 10.1016/J.ANUCENE.2018.05.027.

[19] W. SUN, "A model for hindered diffusion in pores," *Chemical Engineering Research and Design*, vol. 209, pp. 299–310, Sep. 2024, doi: 10.1016/J.CHERD.2024.08.010.

[20] P. MOCZKO, M. J. OLEJNIK, AND J. S. WIĘCKOWSKI, "Thermo-chemical degradation of industrial installations - experimental and numerical technical condition assessment," *Case Studies in Construction Materials*, vol. 17, p. e01685, Dec. 2022, doi: 10.1016/J.CSCM.2022.E01685.

[21] V. B. MØLLER, K.; DAM-JOHANSEN, S. M. G. FRANKAER, AND S. KIIL, "Acid-resistant organic coatings for the chemical industry: a review," *J. Coat. Technol. Res.*, vol. 14, no. 2, pp. 279–306, 2017, doi: 10.1007/s11998-016-9905-2.

[22] L. SUN, C. REN, AND X. L. LUO, "Online control system reconfiguration towards long period energy-saving optimization of heat exchanger networks," *J. Clean. Prod.*, vol. 367, p. 132940, Sep. 2022, doi: 10.1016/J.JCLEPRO.2022.132940.

[23] M. AZIMIFAR, A. MORADIAN, AND A. JAFARIAN, "A numerical investigation on the dynamics of particle deposition and fouling on a vertical falling film pipe," 2024, doi: 10.1016/j.jwpe.2024.105990.

[24] Z. YAN, D. ZHOU, Q. ZHANG, Y. ZHU, AND Z. WU, "A critical review on fouling influence factors and antifouling coatings for heat exchangers of high-salt industrial wastewater," *Desalination*, vol. 553, p. 116504, 2023, doi: 10.1016/j.desal.2023.116504.

[25] L. C. HØGHØJ, D. R. NØRHAVE, J. ALEXANDERSEN, O. SIGMUND, AND C. SCHOUSBOE ANDREASEN, "Topology optimization of two fluid heat exchangers," *Int. J. Heat Mass Transf.*, vol. 163, p. 120543, 2020, doi: 10.1016/j.ijheatmasstransfer.2020.120543.

[26] R. SHEN, Z. FAN, J. XU, B. LI, AND H. WANG, "Quantification and correlation analysis of bubble characteristics and heat transfer performance in direct contact heat exchanger," *Appl. Therm. Eng.*, vol. 236, p. 121856, Jan. 2024, doi: 10.1016/J.APPLTHERMALENG.2023.121856.

[27] S. HOSSEINI *et al.*, "Novel and robust machine learning approach for estimating the fouling factor in heat exchangers," *Energy Reports*, vol. 8, pp. 8767–8776, Nov. 2022, doi: 10.1016/J.EGYR.2022.06.123.

[28] C. SPIEGEL, F. ASELMEYER, W. AUGUSTIN, AND S. SCHOLL, "Quantification method for cleaning-in-place procedures in micro structured equipment," *Food and Bioproducts Processing*, vol. 134, pp. 150–162, Jul. 2022, doi: 10.1016/J.FBP.2022.05.010.

[29] P. HANG, L. ZHAO, AND G. LIU, "Optimal design of heat exchanger network considering the fouling throughout the operating cycle," *Energy*, vol. 241, p. 122913, Feb. 2022, doi: 10.1016/J.ENERGY.2021.122913.

[30] S. LU *et al.*, "Electrochemical effects on carbon steel in circulating cooling water systems: Scaling, corrosion and chemicals synergies," *Journal of Water Process Engineering*, vol. 63, p. 105337, Jun. 2024, doi: 10.1016/J.JWPE.2024.105337.

[31] V. ALAR, I. ŽMAK, B. RUNJE, AND A. HORVATIC, "Development of Models for Prediction of Corrosion and Pitting Potential on AISI 304 Stainless Steel in Different Environmental Conditions," *Int. J. Electrochem. Sci.*, vol. 11, no. 9, pp. 7674–7689, Sep. 2016, doi: 10.20964/2016.09.26.

[32] H. ZHI, P. DONG, K. LI, L. GAO, W. ZHOU, AND H. ZHANG, "Phase field study of pitting corrosion: Electrochemical reactions and temperature dependence," *Comput. Mater. Sci.*, vol. 244, p. 113251, Sep. 2024, doi: 10.1016/J.COMMATSCI.2024.113251.

[33] W. FAES *et al.*, "Corrosion and corrosion prevention in heat exchangers," *Corrosion Reviews*, vol. 37, no. 2, pp. 131–155, Apr. 2019, doi: 10.1515/CORRREV-2018-0054.

[34] W. FAES, J. VAN BAEL, S. LECOMPTE, K. VERBEKEN, AND M. DE PAEPE, "Optimization of heat exchanger design taking corrosion into account," *Thermal Science and Engineering Progress*, vol. 30, p. 101277, May 2022, doi: 10.1016/J.TSEP.2022.101277.

[35] S. KAKAÇ, H. LIU, AND A. PRAMUANJAROENKIJ, *Heat Exchangers : Selection, Rating, and Thermal Design, Fourth Edition*. CRC Press, 2020. doi: 10.1201/9780429469862.

[36] O. W. SIEBERT, Perry's chemical engineers' handbook. Section 25, Materials of construction. McGraw-Hill, 2008.

[37] A. L. SUTTON AND V. C. HOWARD, "The role of porosity in the accommodation of thermal expansion in graphite," *Journal of Nuclear Materials*, vol. 7, no. 1, pp. 58–71, Sep. 1962, doi: 10.1016/0022-3115(62)90194-0.

[38] Z. WANG, Y. XUE, R. WANG, J. WU, Y. ZHANG, AND H. XUE, "Review on crack growth driving force at the tip of stress corrosion cracking in the safe end dissimilar metal welded joint," *Nuclear Engineering and Design*, vol. 429, p. 113609, Dec. 2024, doi: 10.1016/J.NUCENGDES.2024.113609.

[39] T. N. WORDOFA AND P. J. RAMULU, "Gas Metal Arc Welding Input Parameters Impacts on Weld Quality Characteristics of Steel Materials a Comprehensive Exploration," *Manufacturing Technology*, vol. 23, no. 3, pp. 366–379, Jun. 2023, doi: 10.21062/MFT.2023.046.

[40] T. T. HTUT *et al.*, "Fatigue fracture investigation of a tube-to-tubesheet welded joint," *Eng. Struct.*, vol. 283, p. 115908, May 2023, doi: 10.1016/J.ENGSTRUCT.2023.115908.

[41] P. ŽIVNÝ, J. JANSA, M. MĚKUTA, AND P. LUKÁŠOVÁ, "Crack Detection and Monitoring of their Growth in Critical Parts of Steam Pipeline by Electric Potential Drop Method," *Manufacturing Technology*, vol. 25, no. 4, pp. 569–574, Nov. 2025, doi: 10.21062/MFT.2025.046.

[42] A. BAHRAMI, S. H. MOUSAVI ANIJDAN, P. TAHERI, AND M. YAZDAN MEHR, "Failure of AISI 304H stainless steel elbows in a heat exchanger," *Eng. Fail. Anal.*, vol. 90, pp. 397–403, Aug. 2018, doi: 10.1016/J.ENGFAILANAL.2018.04.006.

[43] X. XU, M. LIU, Y. MA, M. AN, AND Y. Ma, "Chaotic vibration characters of a graphite tube with an internal vapor-liquid-solid flow boiling," *Powder Technol.*, vol. 371, pp. 74–82, Jun. 2020, doi: 10.1016/J.POWTEC.2020.05.075.

[44] L. LIU, N. DING, J. SHI, N. XU, W. GUO, AND C. M. L. WU, "Failure analysis of tube-to-tubesheet welded joints in a shell-tube heat exchanger," *Case Stud. Eng. Fail. Anal.*, vol. 7, pp. 32–40, Oct. 2016, doi: 10.1016/J.CSEFA.2016.06.002.

[45] B. A. GORELIK AND M. B. VOSKOBOJNIK, "Flexible highly filled coatings based on PVDF," *J. Fluor. Chem.*, vol. 104, no. 1, pp. 73–77, 2000, doi: 10.1016/S0022-1139(00)00229-3.

[46] D. KUMAR, L. LI, AND Z. CHEN, "Mechanically robust polyvinylidene fluoride (PVDF) based superhydrophobic coatings for self-cleaning applications," *Prog. Org. Coat.*, vol. 101, pp. 385–390, Dec. 2016, doi: 10.1016/J.PORGCOAT.2016.09.003.

[47] "Physical properties – Lauterbach Verfahrenstechnik GmbH." Accessed: Sep. 20, 2024. [Online]. Available: https://lv-soft.net/en/software-products/process-engineering/physical-properties

[48] ENDRESS+HAUSER, "33F | Endress+Hauser." Accessed: Sep. 28, 2024. [Online]. Available: https://www.cz.endress.com/cs/Polni-instrumentace-sita-na-miru/33F?t.tabId=product-overview

[49] JSP Industrial Controls, "Základní hodnoty odporu platinových snímačů teploty Pt100", Accessed: Sep. 28, 2024. [Online]. Available: http://www.jsp.cz/files/c0094kpcz.pdf

[50] "Cerabar M PMP48 | Endress+Hauser." Accessed: Sep. 28, 2024. [Online]. Available: https://www.endress.com/en/field-instruments-overview/PMP48?t.tabId=product-overview

[51] "MathWorks - Maker of MATLAB and Simulink - MATLAB & Simulink." Accessed: Sep. 20, 2024. [Online]. Available: https://www.mathworks.com/

[52] "Forced Circulation Evaporator - JLS USA." Accessed: Feb. 08, 2025. [Online]. Available: https://jlsintl.com/products/evaporation-distillation/evaporation.html